Spectral Trends in the Fluorescence of Single Bacterial Light-Harvesting Complexes: Experiments and Modified Redfield Simulations

Danielis Rutkauskas,* Vladimir Novoderezhkin,† Andrew Gall,‡ John Olsen,§ Richard J. Cogdell,‡ C. Neil Hunter,§ and Rienk van Grondelle*

*Department of Biophysics and Physics of Complex Systems, Division of Physics and Astronomy, Faculty of Sciences, Vrije Universiteit, 1081 HV Amsterdam, The Netherlands; †A. N. Belozersky Institute of Physico-Chemical Biology, Moscow State University, Moscow 119899, Russia; ‡Division of Biochemistry and Molecular Biology, University of Glasgow, Glasgow G12 8QQ, United Kingdom; and §Robert Hill Institute for Photosynthesis, Krebs Institute for Biomolecular Research, and Department of Molecular Biology and Biotechnology, University of Sheffield, Sheffield S10 2TN, United Kingdom

ABSTRACT In this work we present and discuss the single-molecule fluorescence spectra of a variety of species of light-harvesting complexes: LH2 of *Rhodopseudomonas acidophila*, *Rhodobacter sphaeroides*, and *Rhodospirillum molischianum* and LH1 of *Rhodobacter sphaeroides*. The emission spectrum of these complexes varies as a function of time as was described in earlier work. For each type of complex, we observe a pronounced and well-reproducible characteristic relationship between the fluorescence spectral parameters of the peak wavelength, width, and asymmetry. This dependence for the LH2 complexes can be quantitatively explained on the basis of a disordered exciton model by varying the static disorder and phonon coupling parameters. In addition, a correlation of the pigment site energies has to be assumed to interpret the behavior of the LH1 complex.

INTRODUCTION

In purple nonsulfur photosynthetic bacteria, as well as in plants and algae, light-harvesting complexes (LHCs) are mediators of the initial stages of a complex sequence of events involving multiple redox reactions and the creation of a proton gradient across the thylakoid membrane, culminating in the synthesis of carbohydrates in the Calvin cycle. The function of the LHCs is to absorb light energy and funnel it to the reaction center (RC) wherein the turnover and subsequent transfer of electrons to the quinone initiates this chain of events (1).

High-resolution three-dimensional crystal structures of two peripheral LHCs of type 2 (LH2) from the purple bacteria *Rhodopseudomonas* (*Rps.*) *acidophila* and *Rhodospirillum* (*Rs.*) *molischianum* (2–4) show that both complexes consist of two rings of bacteriochlorophyll (BChl) *a* molecules in a protein scaffold and that these are responsible for the absorption bands around 800 and 850 nm, referred to as B800 and B850, respectively. Cryoelectron microscopy has shown that the structure of LH2 of *Rhodobacter* (*Rb.*) *sphaeroides* is similar to that of *Rps. acidophila* (5) whereas LH1 of *Rb. sphaeroides* contains only one pigment ring, with maximum absorption around 875 nm, which is similar to the B850 ring in the LH2 complexes.

The electronic and energy-transfer properties of the LHCs have been successfully described in terms of a model including the excitonic coupling between pigments, static disorder of the pigment electronic transition energies, and dynamic disorder arising from the electronic transition coupling to a phonon bath (6–12). Excitonic coupling leads to the coherent delocalization of a single excitation over a number of pigments in the ring. At the same time the two kinds of disorder destroy the coherence and make the excitation more localized. Most generally, the excitation dynamics in the system of pigments is described using the density matrix formalism. However, in the case where the static disorder prevails over the exciton coupling, this description can be simplified to an incoherent Förster hopping (13); in the opposite case, the excitation evolves due to the exciton relaxation, which is adequately described by the modified Redfield theory (14).

We recently observed fluorescence (FL) spectral diffusion of individual LH2 complexes of *Rps. acidophila* accompanied by changes of the spectral profile shape at room temperature (RT). The FL spectrum was observed to broaden upon a shift of the peak wavelength from the intermediate value. Furthermore, the blue-shifted and intermediate spectral line shapes feature a conventional asymmetry—a marked long wavelength tail—whereas the red-shifted profiles exhibit a clear short wavelength wing. We associate these spectral changes with possible structural deformations of the antenna ring that induce the observed spectral evolution through the protein-pigment interactions. Our results are in line with the earlier room- (15) and low-temperature single-molecule FL experiments (16) that were interpreted in terms of dynamic structural deformations, and they conform to the generally accepted notion of proteins as mobile entities, undergoing a variety of structural deformations on a number of timescales (17).

We quantitatively explained the observed FL profile shapes in the framework of the modified Redfield theory by varying the realization of the static energetic disorder taken

Submitted October 13, 2005, and accepted for publication December 16, 2005.

Address reprint requests to Danielis Rutkauskas, Fax: 31-20-5987999; E-mail: danielis@nat.vu.nl.

0006-3495/06/04/2475/11 $2.00

doi: 10.1529/biophysj.105.075903

from a random Gaussian distribution. An alternative model of partially correlated static disorder in combination with a smaller amount of random disorder was ascertained to interpret low-temperature single-molecule FL excitation experiments (16,18–20). However, such a model results in a weakly allowed lowest excitonic state, which is in contradiction to the observed superradiance of bacterial LHCs at low temperature (21). We recently demonstrated that this model does not reproduce the observed changes of a single LH2 FL spectral shape at RT (V. Novoderezhkin, D. Rutkauskas, and R. van Grondelle, unpublished).

The different FL profile shapes of LH2 of *Rps. acidophila* are due to a subtle interplay between static and dynamic disorder. The static disorder determines the eigenvalues of the exciton states and consequently their splitting and the equilibrium thermal population. It also redistributes the oscillator strength between the states. The dynamic disorder red shifts the exciton components of the emission due to phonon-induced reorganization effects, thus changing the splitting between exciton levels and also broadening them. The higher exciton states are additionally broadened due to dynamic disorder causing the ultrafast relaxation between the exciton states, as observed in time-resolved experiments (22). Thus, the extent to which dynamic disorder influences the spectral profiles of the exciton states depends on the particular realization of the static disorder, which for each exciton level is characterized by the participation ratio (PR), with $PR = \Sigma_n(c_n^k)^4$, where c_n^k are wavefunction amplitudes. Note that the value of PR (dependent on the realization of the static disorder) is the inverse of the coherent delocalization length of the exciton state. In this view, the exciton state localization (determined by the static disorder) is a measure of the effective phonon bath coupling to an exciton state and consequently of the phonon-induced broadening and reorganization shift (V. Novoderezhkin, D. Rutkauskas, and R. van Grondelle, unpublished).

In this study, we further extend our previous work of interpreting the FL spectral profile shape and underlying electronic structure of single LHCs. Here we investigate a variety of different bacterial LHCs for which either crystal structures or accurate structural models exist, enabling the modeling of the FL profile. With this we demonstrate the general applicability of the proposed model for different types of bacterial LHCs.

MATERIALS AND METHODS

LH2 complexes of *Rps. acidophila* 10050 and *Rs. molischianum* DSM120 were purified as described previously (23). LH2 complexes of *Rb. sphaeroides* were purified as in Olsen et al. (24). LH1 membranes were purified according to Olsen et al. (25). The membranes were diluted with a buffer of 1 mM Tris (pH 7.5) and 1 mM EDTA to <5% of sucrose by volume and concentrated by centrifugation for 4 h at 40 krpm in a Beckman (Beckman Coulter, High Wycombe, UK) Ti 45 rotor. The membrane pellet was resuspended in ~1 ml of buffer of 20 mM HEPES (pH 8); and ~500 units of resuspended membranes with outer diameter = 875 were solubilized with 4% β-DDM in buffer of 20 mM HEPES (pH 8) and 5 M NaCl solution added to a final concentration of 155 mM NaCl in 10 ml total volume. The β-DDM was added drip-wise to the resuspended membranes with gentle stirring and left to solubilize for 30 min with stirring at 4°C. The solubilized membranes were centrifuged at 48 krpm for 1 h in a Beckman Ti70.1 rotor to remove any unsolubilized material. The solubilized membranes were then loaded onto a DEAE Sepharose column, 15 ml bed volume, preequilibrated with a solution of 155 mM NaCl, 20 mM HEPES (pH 8), and 0.03% β-DDM, and washed for 90 min at 155 mM NaCl concentration and then at 170 mM NaCl for a further 90 min. The purified complexes were then eluted using a 170–400 mM NaCl salt gradient over 60 min and 4 ml fractions collected for analysis. The purest fractions, as ascertained by the 875:280 nm absorbance ratio, were used in a final purification step on a Superose 200 size exclusion column repreequilibrated to 155 mM NaCl, 20 mM HEPES (pH 8), and 0.03% β-DDM. The fraction at the peak of the elution profile was used for single-molecule spectroscopy.

Stock solutions of all samples were divided into small aliquots and kept at −80°C until thawed and were used only once, thus avoiding repetitive freezing and thawing. For the actual measurement the samples of LH2 of *Rps. acidophila*, *Rb. sphaeroides*, and *Rs. molischianum* were diluted with the buffer of 20 mM Tris (pH 8.0) and 0.1% LDAO. The LH1 of *Rb. sphaeroides* was diluted in a buffer containing 1% of *n*-octyl-β-D-glucopyranoside (β-OG) without buffer exchange. All the samples were flushed and kept in the deoxygenated buffer, the same as the one used for dilution. The oxygen in the buffers used for flushing was removed by means of a three component oxygen scavenger: 100× concentrated water stock solutions containing 20 mg/ml of glucose oxidase and 3.5 mg/ml of catalase were kept at −80°C before use. For deoxygenation 1 ml of stock solution of each component together with 750 mg of glucose were added to 40 ml of buffer, thus fully removing dissolved oxygen. Some measurements were conducted at 5°C to prolong the survival time of less stable species.

Isolated LH2 and LH1 complexes were immobilized on a glass microscope coverslip as described previously (26). The confocal setup utilized to acquire sequences of single-molecule FL spectra is based on a commercial biological microscope described earlier (26). It has an option of 594 nm excitation with a constant power and random polarization He-Ne laser (Melles Griot, Didam, The Netherlands). With this wavelength, the LHCs are excited in their Q_x absorption band allowing the use of the long-pass glass filter RG715 (Edmund Optics, Barrington, NJ) with transmission extended further to the blue as compared to the previously utilized broadband interference filter for 800 nm excitation. The spectral integration time was 1 s. The effect of the objective achromatism on the excitation and signal collection efficiency is compensated for by decollimating the 594 nm beam before the objective.

Spectra were fitted with the skewed Gaussian function to obtain the spectral parameters such as the FL peak (FLP) wavelength, full width at half-maximum (fwhm), and asymmetry or skewness (27). We opt for this function since the FL spectra are intrinsically asymmetric, and a better fit is obtained with the skewed than with the regular Gaussian.

RESULTS

Previously we obtained FL time series of spectra of individual LH2 complexes of *Rps. acidophila* with the aim of observing the spectral dynamics as a signature of possible underlying structural changes. We observed FL spectra with various peak wavelengths and widths, and the characteristic relationship between these spectroscopic parameters was interpreted on the basis of the disordered exciton model of the B850 ring in combination with the Redfield theory that describes excitation relaxation in the excitonic manifold (26,27). Various peak wavelengths were connected to different realizations of static energetic disorder of pigment site

energies that in turn were associated with conformational substates of pigment protein.

In this work, several bacterial LHCs were measured upon 594 nm excitation, using a level of absorbed energy equivalent to 2 μW of 800 nm excitation for LH2 of *Rps. acidophila*. Compared to the previous data analysis, where we investigated averaged single-molecule FL profiles in a few selected peak wavelength intervals, here we consider distributions of peak wavelength and averages of corresponding distributions of spectral width and asymmetry (see below). This results in a characteristic continuous dependency between these spectral parameters, which allows for a more detailed and specific interspecies comparison.

Fig. 1 displays grayscale-coded distributions of spectral fwhm values corresponding to values of FLP for LH2 of *Rps. acidophila*, *Rb. sphaeroides*, and *Rs. molischianum* and for LH1 of *Rb. sphaeroides*. The histograms in Fig. 1 are constructed by fitting all spectra obtained under the same experimental conditions, collecting spectra with their FLP within selected narrow intervals, and building distributions of the corresponding values of fwhm. This is done throughout the range of occurring FLPs so that we obtain distributions of fwhm corresponding to each value of FLP. Fig. 1 is generated by combining all of these distributions and applying a grayscale coding for the frequency of occurrence of fwhms corresponding to a defined FLP interval. Spectra with the intermediate FLP occur more frequently than the shifted spectra. Therefore all histograms feature a bright area corresponding to intermediate single-molecule spectral peak wavelength. LH2 of *Rps. acidophila* and *Rb. sphaeroides* (Fig. 1, *A* and *B*) exhibit pronounced wings corresponding to spectra shifted either to the blue or to the red. These wings are less visible in the case of LH2 of *Rs. molischianum* and LH1 of *Rb. sphaeroides* (Fig. 1, *C* and *D*) due to a lower frequency of spectral jumping of these species with the applied intensity of excitation (the latter three complexes are excited with 594 nm with the intensity equivalent to 2 μW at 800 nm, whereas LH2 of *Rps. acidophila* is excited with 6 μW at 800 nm). A detailed account of possible reasons for the different shape of the averages of these distributions is given bellow.

It appears that there is no one-to-one relationship between the FLP and the fwhm, i.e., individual spectra with the same FLP exhibit a distribution of fwhm values in the range of 20–25 nm. However, averaging of fwhms corresponding to each FLP results in a relation between ⟨fwhm⟩and FLP with a characteristic and fully reproducible shape.

A number of such dependences calculated from data sets obtained for LH2 of *Rps. acidophila* with different excitation intensities is displayed in Fig. 2 *A*. It appears that, notwithstanding the broad distribution in the vertical direction in Fig. 1, the essential features of the ⟨fwhm⟩-FLP relation are very well reproducible between the different data sets. The curve has a conspicuous dip at intermediate values of FLP (corresponding to the maximum of the FLP distribution) and rises on each side. This implies that on average the spectrum is broader for FLP values deviating from the intermediate value around 870 nm. The decline of the curve on each side is an experimental artifact of the FL filter applied to the experiments upon 800 nm excitation, which is apparent from a comparison with the data obtained upon 594 nm excitation (Fig. 2 *B*). At FLPs moderately deviating from 870 nm, the curves are relatively smooth, but they become noisier in the wings due to the limited statistics of the strongly shifted spectral occurrences. The experiment applying intense excitation (1–6 μW) was aimed at probing these occurrences, which may be associated with naturally existing, but less accessible conformational substates of the

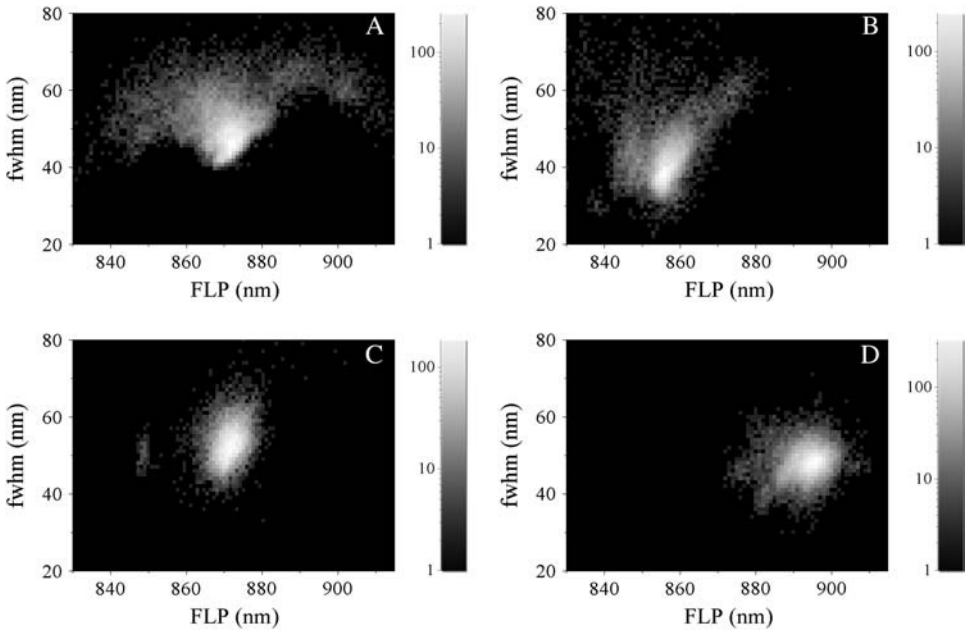

FIGURE 1 Distribution of the occurrences of single-molecule FL spectra with certain fwhm and FLP. The shaded tone of each 1 × 1 nm^2 square in the figure indicates the logarithm of the number of spectra with the FLP and fwhm defined by the position of that square. These histograms resulted from data sets for different species containing (*A*) ~21,000 spectra of LH2 of *Rps. acidophila* obtained with 6 μW at 800 nm excitation at 20°C; (*B*) 15,000 spectra of LH2 of *Rb. sphaeroides* with 6.5 μW at 594 nm; (*C*) 13,000 spectra of LH2 of *Rs. molischianum* with 6 μW at 594 nm at 5°C; and (*D*) 17,000 spectra of LH1 of *Rb. sphaeroides* with 4 μW at 594 nm.

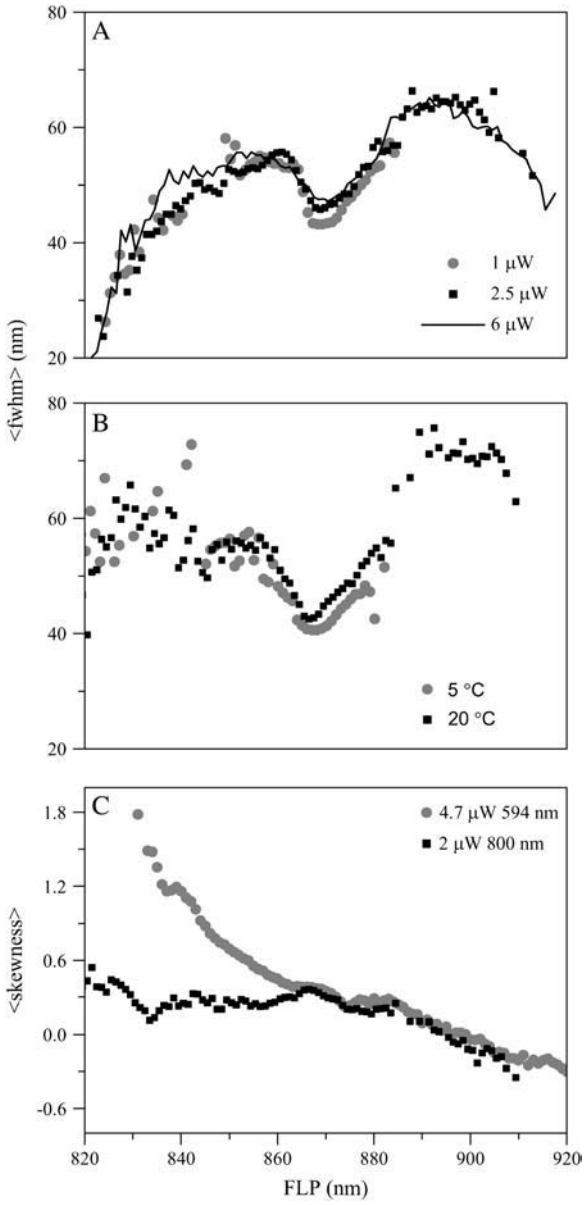

FIGURE 2 LH2 of *Rps. acidophila*. (*Top panel*) ⟨fwhm⟩-FLP dependences at different excitation intensities at 800 nm at 20°C; (*middle panel*) ⟨fwhm⟩-FLP relations at two different temperatures and the same excitation intensity of 4.7 μW at 594 nm; and (*lower panel*) ⟨skewness⟩-FLP curves with two different excitation wavelengths at 20°C.

pigment-protein. Below we will show that in our calculations, similar strongly shifted spectra are generated only in the case when a large number of the static disorder realizations are sampled. This implies that such strongly shifted spectra are not necessarily associated with conformational substates that are difficult to access but that they correspond to rare realizations of the disorder.

With the increased excitation intensity the ⟨fwhm⟩-FLP curve lifts by up to 5 nm (Fig. 2 *A*) for a subset of spectra with peak wavelength between 865 and 875 nm. This change is larger than the experimental error, which is <1 nm as was estimated from the comparison of the data sets obtained with the same experimental conditions (data not shown). This indicates an overall broadening of the spectrum, which is probably due to an increased spectral diffusion that is fast compared to the spectral integration time and which is not observed as a spectral jumping but contributes to the spectral width.

The average spectral width also depends on the temperature of the measurement: spectra at 5°C are generally slightly narrower than those at 20°C (Fig. 2 *B*), which is again probably related to a faster spectral diffusion at 20°C as in the case of the increased excitation intensity.

Since the spectral width does not fully characterize the spectral profile, we also trace the dependence of the average spectral skewness as a function of FLP (Fig. 2 *C*). A simple relationship connects the skewness as a fit parameter of the skewed Gaussian function and the halfwidths at half of the maximum on both sides of the maximum: fit parameter $b = \ln(\delta_2/\delta_1)$, where δ_2 (δ_1) is the long- (short-)wavelength halfwidth. In the case of a slight asymmetry ($b \ll 1$), this yields $b \approx 2(\delta_2 - \delta_1)/\delta$, where $\delta = \delta_2 + \delta_1$ is the fwhm. From a comparison of the ⟨skewness⟩-FLP curves obtained with different excitation wavelengths (for LH2 of *Rps. acidophila* shown in Fig. 2 *C*), it appears that the 800 nm FL filter distorts the experimental FL profiles bluer than 860 nm. At the same time, the two curves overlay very well to the red of 860 nm, demonstrating the reproducibility of this dependency. Generally the spectral asymmetry is rather constant for blue and intermediate FLPs and diminishes for the red-shifted profiles.

The ⟨fwhm⟩-FLP curves for the LH2 of *Rps. acidophila*, *Rb. sphaeroides*, and *Rs. molischianum* and LH1 of *Rb. sphaeroides* are compared in Fig. 3 *A*. The four species were measured with the same equivalent excitation intensity at 594 nm, which enables a direct comparison of the spectral correlations. The curves obtained for LH2 of *Rps. acidophila* and *Rb. sphaeroides* have a similar general shape, although the position of the dip is different along both axes: spectra of *Rb. sphaeroides* with intermediate FLP are narrower and shifted to the blue relative to those of *Rps. acidophila*. The positions of these dips are close to the respective bulk FL maxima. At the same time both curves display a similar rise slope at both sides of the dip.

The curve for LH2 of *Rs. molischianum* has only a small discernible minimum, and it displays a rising wing on the red side but is rather flat in the blue. LH1 of *Rb. sphaeroides* exhibits only a weak dependence of the spectral profile width on the peak wavelength. It should be noted that spectra of LH2 of *Rs. molischianum* with intermediate peak wavelength (~860 nm) are broader than those of any of the remaining three complexes. In that sense LH1 with the most recurring FLP around 890 nm comes second: broader than LH2 of *Rps. acidophila* and *Rb. sphaeroides* and narrower than LH2 of *Rs. molischianum*.

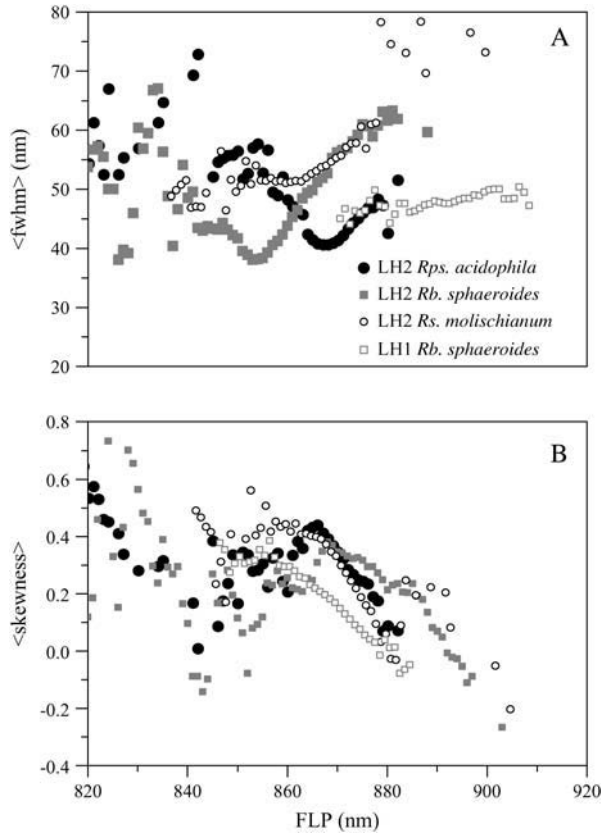

FIGURE 3 (*Top panel*) ⟨fwhm⟩-FLP; (*lower panel*) ⟨skewness⟩-FLP relations for different bacterial LHCs. Different complexes are denoted by LH2 of *Rps. acidophila*, solid circles; *Rb. sphaeroides*, shaded squares; *Rs. molischianum*, open circles; and LH1 of *Rb. sphaeroides*, open squares. All measurements were conducted at 5°C with 594 nm excitation.

Fig. 3 *B* demonstrates the ⟨skewness⟩-FLP dependences for all four LHC species investigated. The curves obtained for LH2 of *Rb. sphaeroides* and *Rs. molischianum* and LH1 of *Rb. sphaeroides* are offset along the FLP axis to match their FLP distribution maxima to that of *Rps. acidophila*. All dependences exhibit the same trend: the spectrum is more symmetric when shifting to the red and features a negative asymmetry at strongly red-shifted FLP values. It also appears that for the same corresponding FLP, LH2 of *Rb. sphaeroides* exhibits the largest asymmetry, *Rps. acidophila* and *Rs. molischianum* are of similar skewness with intermediate magnitude, and LH1 is the most symmetric.

Modeling and discussion

In the following, we do not attempt to interpret the temperature and excitation intensity dependences of the ⟨fwhm⟩-FLP curves since these are rather subtle effects which are much less pronounced than the interspecies variation. However, the curves shown in Fig. 2, *A–C*, demonstrate that in general the dependence of the average spectral fwhm and skewness on the FLP of a single complex is very reproducible for different experimental data sets. Thus in the following we calculate the ⟨fwhm⟩-FLP and ⟨skewness⟩-FLP dependences for different types of complexes with the aim of explaining these general trends.

Modeling the B850 ring

The model of the B850 antenna is the same as used for LH2 of *Rps. acidophila* in previous work (26,27), (V. Novoderezhkin, D. Rutkauskas, and R. van Grondelle, unpublished). In the B850 ring Coulombic interactions between the pigments lead to an excitonic coupling that coherently delocalizes a single excitation over a number of pigments in the ring. The eigenvalues (exciton energy levels) and eigentstates (exciton wave functions) of the system are obtained by diagonalizing the one exciton Hamiltonian and assuming the presence of a random Gaussian static energetic disorder. The spectral profiles of the exciton states are acquired based on the modified Redfield theory (28,29) by taking into account the dynamic disorder associated with the phonon coupling to the electronic transition of a chromophore. A subtle interplay between the two types of disorder determines the overall FL profile as described in the Introduction.

The line-broadening function and the reorganization shift of an exciton state are expressed in terms of a spectral density in the site representation and are proportional to the PR of the exciton state. Compared to the previous work (26,27), this spectral density in the site representation $C(\omega)$ is approximated by a sum of four (instead of just one) Brownian oscillators:

$$C(\omega) = \sum_{m=1-4} 2\lambda_{0m}\frac{\omega\gamma_{0m}}{\omega^2 + \gamma_{0m}^2}, \qquad (1)$$

with characteristic frequencies γ_{0m} = [70 160 450 1200] cm^{-1} and couplings λ_{0m} = [80 170 300 400] cm^{-1}. This form of the spectral density yields more realistic values of phonon-induced line broadening and reorganization shift, since now two Brownian oscillators better account for the low frequency modes and two more take into account the high frequency modes that have not been included previously (at RT the high-frequency peaks are broadened and strongly superimposed, therefore a larger number of Brownian oscillators does not improve the fit). As a result, we have obtained a better quantitative fit of the average FL profiles with different peak wavelengths for LH2 of *Rps. acidophila* (Fig. 4). FL profiles, blue- or red-shifted from the intermediate peak wavelength of 870 nm, are characterized by specific changes of the exciton structure and are accompanied by changes in the spectral width and asymmetry as was described in detail previously (26,27). It is to be noted, however, that the fit of the blue wing (determined by the relaxation-induced broadening) is not perfect. This is connected with the roughness of the relaxation theory. Although modified Redfield is the most advanced among other physical models, it is still too simple. The phonon structure of the line shape in this theory is realistic, being

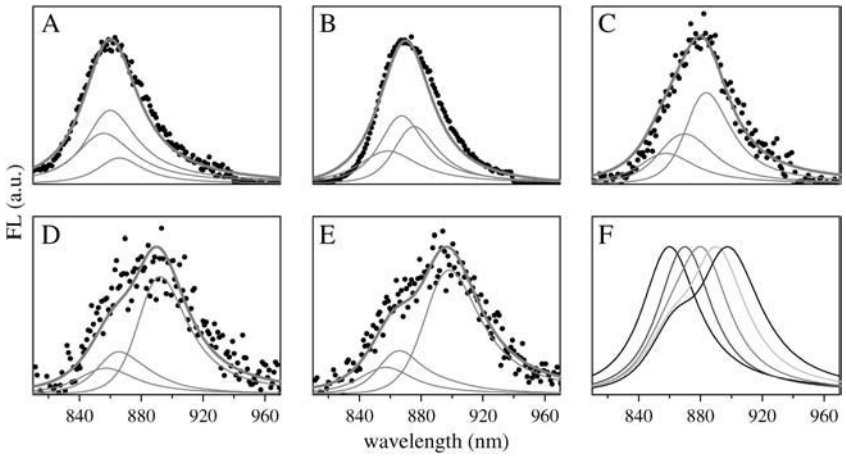

FIGURE 4 FL profiles for the LH2 complex of *Rps. acidophila* at 20°C averaged over realizations with peak wavelengths around (*A*) 860, (*B*) 870, (*C*) 880, (*D*) 890, and (*E*) 900 nm. Experimental data are represented by solid points; calculated spectra (*thick shaded solid lines*) are shown together with the contributions from the three lowest exciton components (*thin shaded solid lines*). The static disorder $\sigma = 350\ \mathrm{cm}^{-1}$. In *F*, calculated FL profiles with different peak positions from (*A–E*) are put together; thermally averaged PR values of 0.1, 0.14, 0.18, 0.22, and 0.27 correspond to the increasingly red-shifted FL profiles.

given by arbitrary strong diagonal exciton-phonon coupling. But the relaxation-induced broadening (due to off-diagonal exciton-phonon coupling) is accounted for perturbatively, i.e., supposing weak interaction with phonons, giving exponential decay and Lorentzian line shapes with unrealistically broad wings. This relaxation-induced broadening is dominant in the blue side of the FL profile (where mostly the short living $k = \pm 1$ states contribute), giving rise to a broad blue wing in the calculated FL spectra. Obviously, this feature is not connected with the choice of the spectral density.

Since the FL spectral profile is determined by the interplay of the static disorder and the phonon-induced shifts and broadenings, we hypothesize that the differences in the ⟨fwhm⟩-FLP and ⟨skewness⟩-FLP curves observed for different species can be reproduced by varying the width of the disorder distribution and the magnitude of the phonon coupling. In the following, we present the variation of the relations between the spectral parameters depending on the static and dynamic disorder. Additionally we investigate the effect of the size of the antenna ring, opening of the ring, and partially correlated disorder due to elliptical deformation. These model calculations are for the B850 ring of the LH2 of *Rps. acidophila* consisting of nine dimeric subunits with the model parameters as specified above unless stated otherwise. Subsequently experimental and calculated ⟨fwhm⟩-FLP and ⟨skewness⟩-FLP dependences are compared for different types of complexes.

Variation of the model parameters

The simulated effects of the static and dynamic energetic disorder on the spectral properties are presented in Fig. 5, *A* and *B*, respectively. It appears that increasing the amount of static disorder, on average, increases the spectral width, flattens the characteristic dip in the ⟨fwhm⟩-FLP dependency at intermediate FLP (~870 nm for the LH2 of *Rps. acidophila*), and shifts it to the red. It also diminishes the spectral asymmetry. Larger dynamic disorder has a similar and even more pronounced effect on the overall spectral width, induces a larger dip in the ⟨fwhm⟩-FLP relationship, and shifts it strongly to the red (Fig. 5 *B*). It also reduces the spectral asymmetry. Thus both types of disorder exert similar effects on the spectral properties except that the larger static disorder flattens the ⟨fwhm⟩-FLP dependency whereas increasing the dynamic disorder makes the dip more noticeable.

The effects of the ring size and deletion of a few dimeric subunits are shown in Fig. 5, *C* and *D*, respectively. Increasing the antenna size from 9 to 16 dimeric subunits somewhat flattens the ⟨fwhm⟩-FLP dependency, shifts it to the blue, and on average narrows down the spectrum noticeably. At the same time the spectral asymmetry alters insignificantly. Opening of the ring by removing 4 dimeric subunits from an antenna containing 16 dimers does not significantly influence either the ⟨fwhm⟩-FLP or ⟨skewness⟩-FLP relationships (Fig. 5 *D*).

The result of the partially correlated disorder due to the elliptical deformation of the ring is presented in Fig. 5 *E*. The applied ellipticity model and its consequences for the electronic structure of the ring are described in more detail in V. Novoderezhkin, D. Rutkauskas, and R. van Grondelle (unpublished). The increased contribution of this disorder lowers the ⟨fwhm⟩-FLP curve and deepens the characteristic minimum, and the general shape of the curve remains similar to that in the absence of the correlation. The spectral asymmetry is lowered although at even larger values of the correlated disorder the skewness of the red-shifted profiles increases.

Having observed the general trends of the ⟨fwhm⟩-FLP and ⟨skewness⟩-FLP relations depending on the model parameters, we may now define the sets of parameters that best reproduce the spectral correlations for different types of complexes.

LH2 of Rps. acidophila

The pigment site energies and interpigment couplings in the B850 antenna of LH2 of *Rps. acidophila* are the same as in

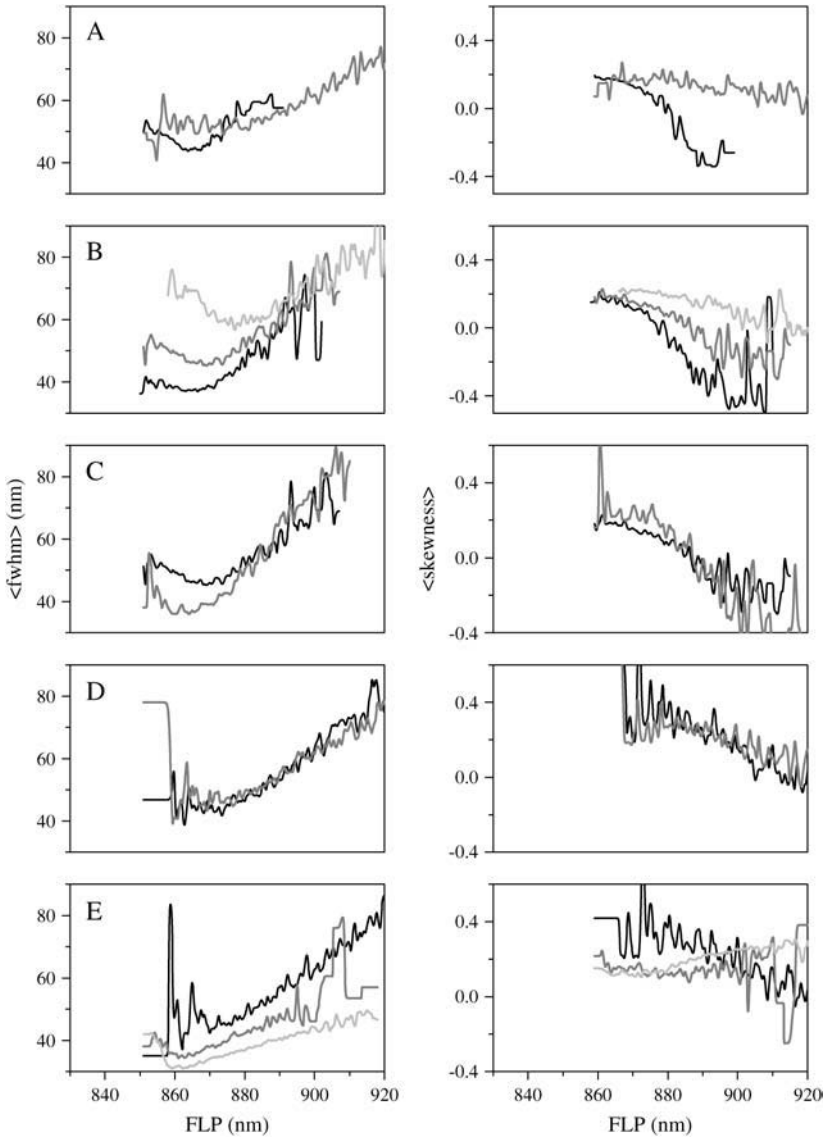

FIGURE 5 Effect of the variation of different model parameters. (*A*) The static disorder, solid curves correspond to $\sigma = 270$ cm^{-1} and shaded curves to $\sigma = 630$ cm^{-1}. (*B*) The dynamic disorder, $\sigma = 370$ cm^{-1}, different curves correspond to the phonon couplings multiplied by a factor of 0.7 (*solid*), 1 (*shaded*), and 1.5 (*light shaded*); (*C*) The antenna size, $\sigma = 370$ cm^{-1}, solid is a ring of nine dimeric subunits, and shaded 16. (*D*) opening of the ring, $\sigma = 630$ cm^{-1}, solid is a full ring of 16 dimeric subunits, and shaded is an incomplete ring of 12 subunits. (*E*) Partially correlated disorder, the ring consists of 16 dimeric subunits, solid corresponds to a ratio of the random static (cm^{-1}) and correlated disorder (cm^{-1}) of 630:0, shaded to 250:330, light shaded to 80:500.

previous work (26,27; V. Novoderezhkin, D. Rutkauskas, and R. van Grondelle, unpublished). Fig. 6 *A* contrasts the experimental and simulated ⟨fwhm⟩-FLP and ⟨skewness⟩-FLP dependences for this complex. The simulation reproduces the experimentally observable trends, although the calculated values of the spectral asymmetry are somewhat lower than the measured ones. This is probably because the relaxation-induced broadening of the $k = \pm 1$ states introduces broad Lorentzian wings to these exciton components. It might be that in reality the relaxation cannot be described by a simple exponential decay (as supposed in a modified Redfield theory) and the actual line shapes are closer to Gaussian.

For the FLP near the intermediate value of 870 nm, the spectra feature a minimal fwhm (43–45 nm) (Fig. 6 *A*) and a regular asymmetry with a sharp blue wing and a broader red tail ($b > 0$) (Figs. 4 *B* and 6 *A*). Such asymmetry is determined by the more intense long wavelength phonon wing in the emission of each of the exciton levels (Fig. 4 *B*).

Blue-shifted spectra exhibit almost the same asymmetry but larger fwhm (up to 52–56 nm) (Fig. 4 *A*). They correspond to a realization of the disorder for which the splitting between the exciton levels is relatively small so that the $k = \pm 1$ levels are populated and this dominates the whole profile. As the emitting levels are mainly the higher energy exciton states, they are broadened due to the predominantly downhill relaxation, giving rise to a broadened overall spectrum.

Red-shifted profiles are determined by a disorder pattern associated with an increased splitting and red shift of the exciton energy levels. The coherence of the exciton states is significantly perturbed; all exciton states and especially the lowest $k = 0$ are strongly localized. An increase of the gap between the exciton states leads to a more populated lowest $k = 0$ state so that even at RT it starts to dominate the overall FL profile. Localization of the lowest state increases its effective coupling to the phonons: the energy level is further

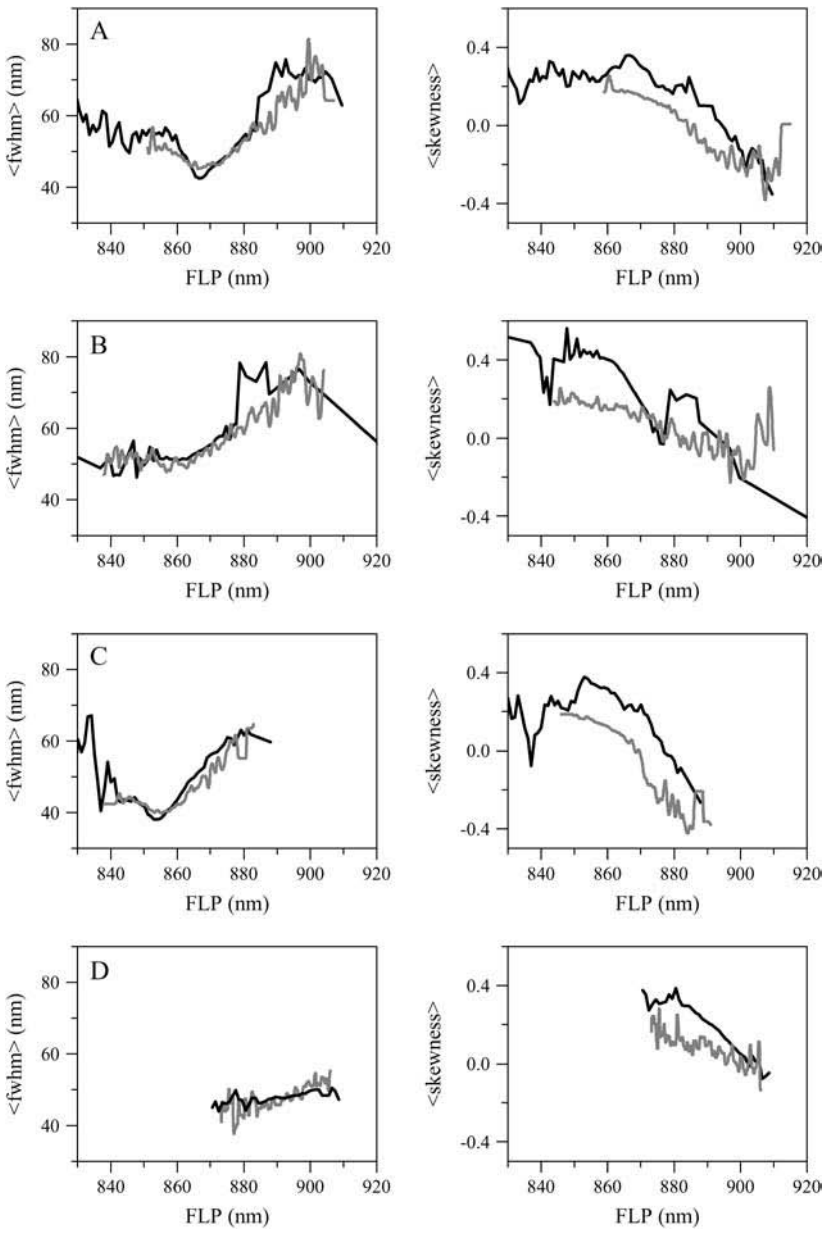

FIGURE 6 Comparison of the experimental and simulated ⟨fwhm⟩-FLP and ⟨skewness⟩-FLP dependences for various complexes. (*A*) LH2 of *Rps. acidophila* at 20°C. The static disorder $\sigma = 350\ \mathrm{cm}^{-1}$. (*B*) LH2 of *Rs. molischianum* at 5°C. Spectral density is the same as for *Rps. acidophila*, but the static disorder is increased to $\sigma = 500\ \mathrm{cm}^{-1}$. (*C*) Analogous to *A*, but for the LH2 of *Rb. sphaeroides* at 5°C. Spectral density is the same as for *Rps. acidophila*, but the exciton-phonon couplings λ_{0m} are reduced by a factor of 1.2 and the static disorder is decreased to $\sigma = 300\ \mathrm{cm}^{-1}$. (*D*) LH1 of *Rb. sphaeroides* at 5°C. The ring contains 32 pigments, the spectral density is the same as for *Rps. acidophila*, but the exciton-phonon couplings λ_{0m} are increased by a factor of 1.28, and site energies of every fifth pigment are obtained from a Gaussian distribution of the width of 380 cm^{-1}. The experimental data are represented by solid and the calculation by shaded curves.

broadened and additionally red-shifted due to reorganization effects. As a result, the FL profile, with the FLP value increasing from 890 to 900 nm, broadens and even changes the sign of the asymmetry parameter. Such extremely red-shifted spectra have a shoulder around 860 nm (seen both in the experimental and calculated spectra, Fig. 4, *D* and *E*) due to contributions from the higher exciton states, whereas the intense emission from the lowest exciton state determines the peak at 890–900 nm. Note that individual exciton components still have their ''normal'' asymmetry; but the whole FL profile becomes sharper in the red, giving rise to a negative value of the skewness starting from FLP of 885 nm in the calculation and 890–895 nm in the measurement.

LH2 of Rs. molischianum

For LH2 of *Rs. molischianum* the pigment-pigment couplings are the same as those in the previous modeling of this complex (9): the energies of the $1\alpha1\beta$, $1\beta2\alpha$, $1\alpha2\alpha$, $1\beta2\beta$, and $1\alpha2\beta$ interactions are $+273$, $+249$, -38, -26, and $+10$ cm^{-1}, respectively.

The site energies are blue-shifted by 10 nm relative to those of LH2 of *Rps. acidophila* to reproduce the overall shift of the bulk absorption spectrum. We found that the differences between LH2 of *Rps. acidophila* and *Rs. molischianum* in interpigment coupling and/or antenna size (nine and eight dimeric subunits, respectively) do not significantly influence the structure of the lowest exciton band. Instead, the broader FL spectrum of *Rs. molischianum* (Fig. 3 *A*) could be

explained by an increase of the static and/or dynamic (phonon-induced) disorder. As was shown above, the increase in the static disorder generally broadens the FL spectrum and diminishes the dip in the ⟨fwhm⟩-FLP relationship. Thus, the ⟨fwhm⟩-FLP and ⟨skewness⟩-FLP dependences could be reproduced with the same spectral density as for the *Rps. acidophila* but with the static disorder distribution broadened from 350 to 500 cm^{-1} (Fig. 6 *B*).

The broadened static disorder distribution produces fewer realizations of the delocalized exciton structure (the ''blue'' realizations in the case of LH2 of *Rps. acidophila*). Generally speaking this has a dramatic effect on the dynamics of the most delocalized blue-shifted realizations. The rate of the relaxation between the exciton states (proportional to their delocalization length) is significantly reduced, diminishing the relaxation-induced broadening of the blue-shifted FL profiles. The result is a flatter ⟨fwhm⟩-FLP dependence at shorter wavelengths (compare Figs. 6, *A* and *B*).

A second consequence of the smaller delocalization is an increase in the effective phonon coupling to the exciton states. This lifts the ⟨fwhm⟩-FLP dependence so that the ⟨fwhm⟩ corresponding to the intermediate FLP value of 860 nm is 50–52 nm for *Rs. molischianum* instead of 43–45 nm at ~870 nm for *Rps. acidophila*.

LH2 of Rb. sphaeroides

In the model calculations above, it was demonstrated that the decrease of the static or dynamic disorder has a similar effect on the average spectral width, but for the former the dip in the ⟨fwhm⟩-FLP dependency increases whereas it decreases for the latter. The curve can be lowered by scaling both types of disorder simultaneously, thus preserving its general shape. Indeed, the data for LH2 of *Rb. sphaeroides* can be explained by proportionally reducing the values of the static and dynamic disorder for LH2 of *Rps. acidophila* (i.e., the site inhomogeneity σ and the couplings λ_{0m}) by a factor of 1.2 (Fig. 6 *C*). The average FLP was adjusted by introducing an 8 nm blue shift of the unperturbed site energies of *Rb. sphaeroides* compared to *Rps. acidophila*. The character of the ⟨fwhm⟩-FLP and ⟨skewness⟩-FLP dependences is the same as for the LH2 of *Rps. acidophila* (compare Figs. 6, *A* and *C*), which is related to the fact that the ratio between the static and dynamic disorder values is the same for both species. At the same time, the decrease of the absolute value of the static disorder results in a generally narrower FL spectral profile for LH2 of *Rb. sphaeroides*.

LH1 of Rb. sphaeroides

Within the range of the observable FLP values (870–910 nm), the ⟨fwhm⟩ of the LH1 complex varies less than for any of the investigated complexes. This dependence is to some extent similar to that of the LH2 of *Rps. molischianum*: the ⟨fwhm⟩ is rather constant at relatively blue FLPs for both complexes. This resemblance probably stems from the similarity of the binding pocket of the B850 (B870) BChls *a* in the two complexes (30), implying a similar character of the protein-pigment interactions determining the electronic structure and the associated FL spectrum of the ring (31,32). Thus, the general trend of only a weakly rising ⟨fwhm⟩-FLP relationship can be obtained by increasing the static disorder value as in the case of LH2 of *Rs. molischianum*. At the same time other factors that were found to influence the spectral properties of the antenna have to be considered for a better fit.

The LH1 complex has been recognized to be remarkably heterogeneous, exhibiting a variety of different shapes and ring sizes, especially in the absence of the RC complex which is normally enclosed by LH1 (33). It is not unreasonable to expect that even an additional purification step with the size-exclusion column does not result in a completely homogeneous sample consisting of particles of the same ring size and/or shape. Thus what we observe may correspond to the spectral response of a mixture of different structural fractions. However, it was demonstrated above that the variation of the B850 ring size from 9 to 16 dimeric subunits increases the slope of the ⟨fwhm⟩-FLP> curve at the edges (Fig. 5 *C*), whereas removal of up to 4 dimeric subunits from the intact ring of 16 dimers does not noticeably affect the spectral properties (Fig. 5 *D*).

Introducing the partially correlated disorder due to the elliptical deformation decreases the slope of the dependence on the red side but significantly lowers the curve and introduces its steeper rise in the blue (Fig. 5 *E*). In addition the ⟨skewness⟩-FLP dependence becomes rather flat, which is unlike the measured relationship. Thus it appears that making allowances for either the larger size of the LH1 ring or its opening or elliptical deformation do not improve the overlay of the measurement and simulation.

We also investigated the possibility of the correlation of the site energies of a certain number of neighboring pigments. Fig. 6 *D* demonstrates the best fit between the experimental and calculated curves in the case of the correlation radius of five pigments, which implies that the site energies of every fifth pigment in the ring are obtained at random from the Gaussian distribution whereas the site energies of the intermediate sites are calculated from a cubic spline dependence connecting those points. Such refinement of the model allows us to reproduce a very slight rise of the FLP-⟨fwhm⟩ dependence and the descent of the FLP-⟨skewness⟩relationship.

It is possible that after some modification the model will allow us to further refine the interpretation of the behavior of the LHCs. This could be a more complicated heterogeneity of the site energies in the case of LH1—an alternative spectral density function taking into account the coupling to the low-frequency vibrations that have been determined experimentally (34), or generalization of the modified Redfield approach by including 1–2 vibrational coordinates

yielding different relaxation dynamics and different spectral line shapes. However, these possibilities deserve a separate study and will be explored in a subsequent article.

CONCLUSIONS

We have obtained collections of FL spectra of individual bacterial LHCs of several different types. Every data set exhibited a distribution of the spectral peak wavelength and a corresponding spectral width and asymmetry. Each species exhibited a characteristic dependence between the average spectral width and asymmetry and the corresponding peak wavelength that was highly reproducible for different data sets of the same type of complex. Ensemble averaging was circumvented by acquiring spectra of individual complexes, which allowed the direct comparison of the experimental and simulated spectra as calculated with different realizations of static disorder to reproduce the occurrence of different spectral peak wavelengths. By varying the amount of the static disorder and the strength of the phonon coupling to the electronic transitions, the same basic model of a disordered excitonically coupled pigment ring quantitatively reproduced the dependences between the spectral parameters for the LH2 ring of different complexes. At the same time, a correlation between the pigment site energies has to be assumed to interpret the corresponding dependences for the LH1 complex.

This research was supported by the Netherlands Organization for Scientific Research. J.O., C.N.H., A.G., and R.J.C. gratefully acknowledge the support of the Biotechnology and Biological Sciences Research Council UK. V.N. was supported by Russian Foundation for Basic Research grant 02-04-48779.

REFERENCES

1. Whitmarsh, J., and J. A. Govindjee. 1999. The photosynthetic process. *In* Concepts in Photobiology: Photosynthesis and Photomorphogenesis. G. Singhal, G. Renger, S. Sopory, K.-D. Irrgang, and Govindjee, editors. Narosa Publishers, New Delhi. 11–51.
2. Koepke, J., X. C. Hu, C. Muenke, K. Schulten, and H. Michel. 1996. The crystal structure of the light-harvesting complex II (B800–850) from *Rhodospirillum molischianum*. *Structure*. 4:581–597.
3. McDermott, G., S. M. Prince, A. A. Freer, A. M. Hawthornthwaite, M. Z. Papiz, R. J. Cogdell, and N. W. Isaacs. 1995. Crystal structure of an integral membrane light-harvesting complex from photosynthetic bacteria. *Nature*. 374:517–521.
4. Papiz, M. Z., S. M. Prince, T. Howard, R. J. Cogdell, and N. W. Isaacs. 2003. The structure and thermal motion of the B800–850 LH2 complex from *Rps. acidophila* at 2.0 Å resolution and 100 K: new structural features and functionally relevant motions. *J. Mol. Biol*. 326:1523–1538.
5. Walz, T., S. J. Jamieson, C. M. Bowers, P. A. Bullough, and C. N. Hunter. 1998. Projection structures of three photosynthetic complexes from *Rhodobacter sphaeroides*: LH2 at 6 Å LH1 and RC-LH1 at 25 Å. *J. Mol. Biol*. 282:833–845.
6. Alden, R. G., E. Johnson, V. Nagarajan, W. W. Parson, C. J. Law, and R. J. Cogdell. 1997. Calculations of spectroscopic properties of the LH2 bacteriochlorophyll-protein antenna complex from *Rhodopseudomonas acidophila*. *J. Phys. Chem. B*. 101:4667–4680.
7. Hu, X. C., T. Ritz, A. Damjanovic, and K. Schulten. 1997. Pigment organization and transfer of electronic excitation in the photosynthetic unit of purple bacteria. *J. Phys. Chem. B*. 101:3854–3871.
8. Novoderezhkin, V., R. Monshouwer, and R. van Grondelle. 1999. Exciton (de)localization in the LH2 antenna of *Rhodobacter sphaeroides* as revealed by relative difference absorption measurements of the LH2 antenna and the B820 subunit. *J. Phys. Chem. B*. 103:10540–10548.
9. Novoderezhkin, V., M. Wendling, and R. van Grondelle. 2003. Intra- and interband transfers in the B800–B850 antenna of *Rhodospirillum molischianum*: Redfield theory modeling of polarized pump-probe kinetics. *J. Phys. Chem. B*. 107:11534–11548.
10. Scholes, G. D., and G. R. Fleming. 2000. On the mechanism of light harvesting in photosynthetic purple bacteria: B800 to B850 energy transfer. *J. Phys. Chem. B*. 104:1854–1868.
11. van Grondelle, R., and V. Novoderezhkin. 2001. Dynamics of excitation energy transfer in the LH1 and LH2 light-harvesting complexes of photosynthetic bacteria. *Biochemistry*. 40:15057–15068.
12. Wu, H. M., M. Rätsep, I. J. Lee, R. J. Cogdell, and G. J. Small. 1997. Exciton level structure and energy disorder of the B850 ring and the LH2 antenna complex. *J. Phys. Chem. B*. 101:7654–7663.
13. Förster, T. 1965. Action of light and organic crystals. *In* Modern Quantum Chemistry. Istanbul Lectures. Part III. O. Sinannoglu, editor. Academic Press, New York. 93–137.
14. Redfield, A. G. 1965. The theory of relaxation processes. *Adv. Magn. Reson*. 1:1–32.
15. Bopp, M. A., A. Sytnik, T. D. Howard, R. J. Cogdell, and R. M. Hochstrasser. 1999. The dynamics of structural deformations of immobilized single light-harvesting complexes. *Proc. Natl. Acad. Sci. USA*. 96:11271–11276.
16. van Oijen, A. M., M. Ketelaars, J. Köhler, T. J. Aartsma, and J. Schmidt. 2000. Spectroscopy of individual light-harvesting 2 complexes of *Rhodopseudomonas acidophila*: diagonal disorder, intercomplex heterogeneity, spectral diffusion, and energy transfer in the B800 band. *Biophys. J*. 78:1570–1577.
17. Frauenfelder, H., S. G. Sligar, and P. G. Wolynes. 1991. The energy landscapes and motions of proteins. *Science*. 254:1598–1603.
18. Ketelaars, M., A. M. van Oijen, M. Matsushita, J. Köhler, J. Schmidt, and T. J. Aartsma. 2001. Spectroscopy on the B850 band of individual light-harvesting 2 complexes of *Rhodopseudomonas acidophila* I. Experiments and Monte Carlo simulations. *Biophys. J*. 80:1591–1603.
19. Matsushita, M., M. Ketelaars, A. M. van Oijen, J. Köhler, T. J. Aartsma, and J. Schmidt. 2001. Spectroscopy on the B850 band of individual light-harvesting 2 complexes of *Rhodopseudomonas acidophila* II. Exciton states of an elliptically deformed ring aggregate. *Biophys. J*. 80:1604–1614.
20. van Oijen, A. M., M. Ketelaars, J. Köhler, T. J. Aartsma, and J. Schmidt. 1999. Unraveling the electronic structure of individual photosynthetic pigment-protein complexes. *Science*. 285:400–402.
21. Monshouwer, R., M. Abrahamsson, F. van Mourik, and R. van Grondelle. 1997. Superradiance and exciton delocalization in bacterial photosynthetic light-harvesting systems. *J. Phys. Chem. B*. 101:7241–7248.
22. Novoderezhkin, V., R. Monshouwer, and R. van Grondelle. 1999. Disordered exciton model for the core light-harvesting antenna of *Rhodopseudomonas viridis*. *Biophys. J*. 77:666–681.
23. Gall, A., and B. Robert. 1999. Characterization of the different peripheral light-harvesting complexes from high- and low-light grown cells from *Rhodopseudomonas palustris*. *Biochemistry*. 38:5185–5190.
24. Olsen, J. D., B. Robert, A. Siebert, P. A. Bullough, and C. N. Hunter. 2003. Role of the C-terminal extrinsic region of the alpha polypeptide of the light-harvesting 2 complex of *Rhodobacter sphaeroides*: a domain swap study. *Biochemistry*. 42:15114–15123.
25. Olsen, J. D., G. D. Sockalingum, B. Robert, and C. N. Hunter. 1994. Modification of a hydrogen bond to a bacteriochlorophyll a molecule in the light-harvesting 1 antenna of *Rhodobacter sphaeroides*. *Proc. Natl. Acad. Sci. USA*. 91:7124–7128.

26. Rutkauskas, D., V. Novoderezhkin, R. J. Cogdell, and R. van Grondelle. 2005. Fluorescence spectroscopy of conformational changes of single LH2 complexes. *Biophys. J.* 88:422–435.

27. Rutkauskas, D., V. Novoderezkhin, R. J. Cogdell, and R. van Grondelle. 2004. Fluorescence spectral fluctuations of single LH2 complexes from *Rhodopseudomonas acidophila* strain 10050. *Biochemistry.* 43:4431–4438.

28. Mukamel, S. 1995. Principles of Nonlinear Optical Spectroscopy. Oxford University Press, New York.

29. Zhang, W. M., T. Meier, V. Chernyak, and S. Mukamel. 1998. Exciton-migration and three-pulse femtosecond optical spectroscopies of photosynthetic antenna complexes. *J. Chem. Phys.* 108:7763–7774.

30. Germeroth, L., F. Lottspeich, B. Robert, and H. Michel. 1993. Unexpected similarities of the B800–850 light-harvesting complex from *Rhodospirillum molischianum* to the B870 light-harvesting complexes from other purple photosynthetic bacteria. *Biochemistry.* 32:5615–5621.

31. Robert, B., R. J. Cogdell, and R. van Grondelle. 2003. The light-harvesting system of purple bacteria. *In* Light-Harvesting Antennas in Photosynthesis. B. R. Green and W. W. Parson, editors. Kluwer Academic Publishers, Dordrecht, The Netherlands. 169–194.

32. Cogdell, R. J., T. D. Howard, N. W. Isaacs, K. McLuskey, and A. T. Gardiner. 2002. Structural factors which control the position of the Q_y absorption band of bacteriochlorophyll a in purple bacterial antenna complexes. *Photosynth. Res.* 74:135–141.

33. Bahatyrova, S., R. N. Frese, K. O. van der Werf, C. Otto, C. N. Hunter, and J. D. Olsen. 2004. Flexibility and size heterogeneity of the LH1 light harvesting complex revealed by atomic force microscopy—functional significance for bacterial photosynthesis. *J. Biol. Chem.* 279: 21327–21333.

34. Novoderezhkin, V., R. Monshouwer, and R. van Grondelle. 2000. Electronic and vibrational coherence in the core light-harvesting antenna of *Rhodopseudomonas viridis*. *J. Phys. Chem. B.* 104:12056–12071.